Available online at www.sciencedirect.com
ScienceDirect
Materials Chemistry and Physics 109 (2008) 448–454
MATERIALS CHEMISTRY AND PHYSICS
www.elsevier.com/locate/matchemphys

On the nature of goethite, Mn-goethite and Co-goethite as supports for gold nanoparticles

Betiana C. Campo [a], Olivier Rosseler [b], Mariana Alvarez [c], Elsa H. Rueda [c], María A. Volpe [a,*]

[a] *PLAPIQUI, Camino Carrindanga km7, 8000 Bahia Blanca, Argentina*
[b] *LMSPC, UMR 7515 du CNRS, ECPM, ULP, 25, rue Becquerel, 67087 Strasbourg Cedex 2, France*
[c] *Universidad Nacional del Sur, Avda. Alem 1253, 8000 Bahia Blanca, Argentina*

Received 21 August 2007; received in revised form 5 December 2007; accepted 7 December 2007

Abstract

Mn- and Co-substituted goethite (α-MnFeOOH and α-CoFeOOH) and pure goethite (α-FeOOH) were studied as supports for gold catalysts. The textural properties of these solids were studied by N_2/77 K adsorption. Mn and Co substitutions gave rise to an increase of the specific surface area, as measured by BET equation. A DTA study indicated that the thermal stability of goethite was increased by Mn and Co incorporation. XRD analysis showed that both Mn and Co strongly modified goethite cell parameters, giving rise to an increase of the reducibility of both substituted oxyhydroxides, as measured by TPR. Three different samples were obtained by anchoring gold by direct anion exchange (DAE) method from $HAuCl_4$: Au/α-FeOOH, Au/α-CoFeOOH and Au/α-MnFeOOH. FT-IR indicated that gold species were attached to OH goethite groups, while TEM analysis demonstrated that gold particles were in the nanometric range for all the samples. On pure goethite gold particles size distribution was relatively narrow, while for the cases of Au/α-MnFeOOH and Au/α-CoFeOOH a wide crystal size distribution were obtained. It is concluded that α-MnFeOOH and α-CoFeOOH are better supports for the gold particles since reducibility, thermal stability and specific surface area are higher than in the case of pure α-FeOOH.

Keywords: Goethite; Supported gold catalysts; Mn-goethite; Co-goethite; Gold nanoparticles

1. Introduction

The transcendental discoveries made by Hutchings [1] and Haruta et al. [2] in the 1980s regarding the surprising activity of gold catalysts in the acetylene hydrochlorination and CO oxidation at low temperature initiated the *golden age* on the heterogeneous catalysis field [3].

The break point in the history of gold as catalytic material was the synthesis of supported nanoparticles, since within this range gold losses its noble character. Supported gold nanoparticles were successfully employed in diverse reactions [4–7].

A huge number of studies has been focused on different oxides as carriers for gold nanoparticles. However, there are many unexplored systems which could be supports for efficient gold-based catalysts. One of these systems is the substituted Fe oxyhydroxides. Although gold supported on iron oxide has been studied as catalysts in water-gas shift reaction [8,9], selective hydrogenation reactions [10], and the direct synthesis of hydrogen peroxide from H_2 and O_2 [11,12], to our knowledge substituted iron oxides have been never studied as supports for gold.

Synthetic goethite (α-FeOOH) can incorporate di-, tri, and tetravalent metal species as Al, Cr, Cd, Co, Cu, Pb, V, Mn and Zn. It has been shown that these isomorphous substitutions modify the structural parameters of the solid as well as its chemical properties [13–17]. The modification of the reducibility of the goethite [18] and the change in the surface area of the solid [19] due to the substitution should be underlined since these characteristics are significant for developing new gold catalysts. For example, Milone et al. [20,21] studied the selective oxidation of *o*-hydroxylbenzylalcohol over gold supported on iron oxyhydroxides and they observed a strong influence of the reducibility of the catalyst on their catalytic properties (specific activity).

* Corresponding author. Tel.: +54 291 4861666; fax: +54 291 4861600.
E-mail address: mvolpe@plapiqui.edu.ar (M.A. Volpe).

0254-0584/$ – see front matter © 2007 Elsevier B.V. All rights reserved.
doi:10.1016/j.matchemphys.2007.12.014

In this context the present work is focused on goethite and Mn- and Co-substituted goethite as supports for gold nanoparticles. Au/α-FeOOH, Au/α-MnFeOOH and Au/α-CoFeOOH systems were prepared by fixing gold by direct anion exchange (DAE) procedure from $HAuCl_4$. This method of preparation was selected since it is based upon a direct anion exchange of the gold species for the hydroxyl groups of the support. The samples were characterized by X-ray diffraction, differential thermal analysis, and FT-IR spectroscopy to study the influence of Mn and Co substitution on the physicochemical properties of goethite. Besides, N_2/77 K isothermal adsorption was carried out to determine the textural properties of the different samples (specific surface area and pore volume). Transmission electron microscopy was employed to determine the effect of metal substitution on gold particle size.

2. Experimental

2.1. Synthesis of the supports

Samples of goethite and Me-goethites (Me = Co and Mn) were prepared as described by Stiers and Schwertmann [22] with some modifications introduced by Schwertmann and Cornell [23]. Ferrihydrite was precipitated by adding a 2 mol dm^{-3} NaOH solution to a Fe(III) solution (for pure goethite) and a Fe(III) and Me(II) nitrate solution until the ratio Me/OH$^-$ was 0.076, in order to reach a Me-substitution of 0.10 mol mol^{-1}. For both samples the initial concentration of the solution was 0.53 mol dm^{-3}. The precipitates thus obtained were washed twice with bidistilled water and centrifuged. After this treatment, the samples were held for 15 days at 60 °C in closed polyethylene flasks containing 0.3 mol dm^{-3} NaOH. After aging, the materials were washed with bidistilled water until the conductivity of the filtered solution was similar to that of bidistilled water. The remaining solids were dried at 40 °C and gently crushed. The Mn and Co containing samples were named as α-MnFeOOH and α-CoFeOOH.

2.2. Supporting gold

Gold was fixed to goethite and Me-goethites by the DAE method [24]. Aqueous solutions of $HAuCl_4$ of concentration 1×10^{-3} mol dm^{-3} were prepared in order that a final Au loading of 2 wt% was obtained. The solution adjusted at pH 3 was heated to 70 °C and the powdered support was added. Ammonia as aqueous solution (4 mol dm^{-3}) was adding to the suspension in order to remove the chlorine species. Approximately 20 min later the suspension was filtered, exhaustively washed with distilled water and dried overnight in an oven at 100 °C.

2.3. Sample characterization

Metal contents in the original solids were determined dissolving 20 mg of each sample in HCl 6 mol dm^{-3} using a GBC, Model B-932 atomic absorption spectrometer.

X-ray diffraction patterns have been recorded in a Siemens D5000 diffractometer using a Cu Kα radiation and 2 sets of 1° Soller slits and a graphite monochromator. The data were collected in the 2θ range: 15.800–140.000°, the scanning step was 0.025°, 4969 points were measured with a counting time of 20 s per point.

Gold particle size was measured by transmission electron microscopy (TEM) on a Jeol 100 CX2 (Tokyo, Japan) apparatus.

Nitrogen adsorption isotherms at 77 K were obtained on a NOVA 1200e equipment. The samples were evacuated at 120 °C for 2 h prior to the measurements. The surface areas of the samples were estimated by the conventional BET method [25].

Differential thermal analyses (DTA) were performed using a DTA-50 Shimadzu instrument. Samples of approximately 5 mg were heated in a N_2 atmosphere to 500 °C with a heating rate of 10 °C min^{-1}.

FT-IR spectra were taken over samples supported on KBr disks, in the range 250–4000 cm^{-1}, using a Nicolet 20DXB FT-IR Spectrometer.

Temperature-programmed reduction (TPR) experiments were carried out in a conventional apparatus. Approximately 100 mg of the samples were placed in a glass reactor and calcined at 100 °C for 1 h under air flow. Subsequently, air was purged under Ar flow and the sample was cooled down. Then, samples were heated from room temperature to 500 °C at a ramp rate of 10 °C min^{-1}, under 5 vol% H_2/Ar, with a constant flow rate of 20 cm^3 min^{-1}. A TCD detector monitored the rate of hydrogen consumption. The area of the resulting peaks was integrated numerically, yielding the total hydrogen uptake volume.

3. Results and discussion

3.1. Characterization of goethite and substituted goethite

In Table 1 the chemical composition of α-FeOOH, α-CoFeOOH and α-MnFeOOH are reported. Taking into account the metal concentrations shown in Table 1, the formulation of the samples is α-$Mn_{0.09}Fe_{0.91}$OOH and α-$Co_{0.06}Fe_{0.94}$OOH. The extent of the Mn substitution is higher than that corresponding to Co.

Fig. 1 presents the XRD patterns corresponding to goethite and Mn- and Co-substituted goethite. It can be observed that the goethite structure is present for the three cases.

Goethite presents the orthorhombic *Pbnm* space group, the unit cell contains four groups Me, O, OH. The structure is based on a HCP packing of oxygen and hydroxide ions where half of

Table 1
Chemical composition and textural properties of goethite, substituted goethite and Au/goethite

Sample	%Co or Mn[a]	%Au[a]	S BET[b] (m^2 g^{-1})	V_{micro}[c]	H_R/H_T[d]	H_R/H_T[e]
G_0	0	–	27.5	0.11	0.56	0.96
G_{Mn}	5.3	–	42.1	0.14	0.63	1.12
G_{Co}	3.5	–	87.3	0.22	0.48	0.96
Au/G_0	0	0.98	27.5		1.34	1.51
Au/G_{Mn}	5.3	2.00	88.0		1.32	1.72
Au/G_{Co}	9.5	1.98	51.1		1.30	2.31

[a] Metal concentration expressed as % (w/w).
[b] Specific surface area (m^2 g^{-1}).
[c] Micropore volume (cm^3 g^{-1}).
[d] Ratio between the real and theoretical consumption of hydrogen (peak α) considering the stoichiometric reduction of goethite to magnetite.
[e] Ratio between the real and theoretical consumption of hydrogen at 500 °C (peaks α, β and γ) considering the stoichiometric reduction of goethite magnetite.

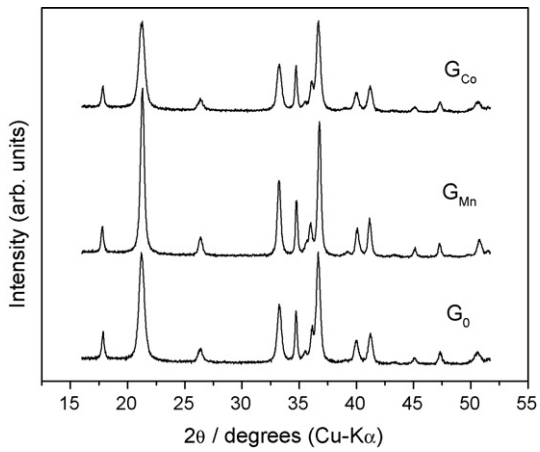

Fig. 1. XRD patterns of α-FeOOH (G_0), α-MnFeOOH (G_{Mn}) and α-CoFeOOH (G_{Co}).

the octahedral sites are filled with metal ions. Fig. 2 depicts the goethite structure which may be described as a series of double row octahedra that run parallel to [0 0 1]; these double rows are separated by vacant double rows. Each octahedron in the double row shares two oxygen atoms from the same edge with two different octahedra from the same double row, also each octahedron shares two corners with two polyhedra from a neighboring double row. This structure determines the presence of three different Me–Me distances. In each double row the polyhedra joined by the edges determine the Me–Me distances E and E', where E' coincides with the c cell parameter (see Fig. 2). The connection between double rows determines a different Me–Me distance, named a DC distance.

A Rietveld refinement of XRD data corresponding to Fig. 1 was carried out. The results showed a decrease in the a and c parameters and an increase in b parameter in the case of α-MnFeOOH. The distortion in cell parameters due to Mn substitution is assigned to the Jahn Teller effect corresponding to Mn(III), with a d^4 ion configuration. On the other hand, upon substitution with Co a clear decrease in the unit cell parameters was observed suggesting that this cation is incorporated in the goethite particles in a trivalent state rather than

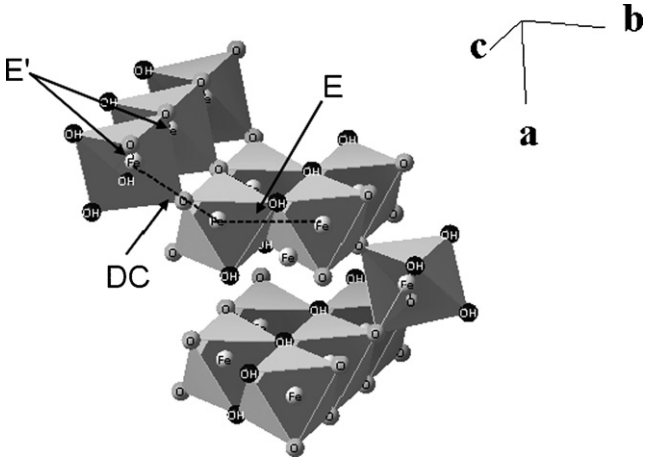

Fig. 2. Goethite structure showing the polyhedra linkages.

the divalent one, since the ionic radii for Co(III) cations in high-spin configuration (0.525 Å) is lower than that of high-spin Fe(III) (0.650 Å) [26]. These results are in agreement with previous works [27,28]. Particle morphologies were studied by SEM analysis. The micrographs corresponding to α-FeOOH, α-MnFeOOH and α-CoFeOOH are shown in Fig. 3. It can be observed that all samples present an acicular habit, with an enlargement of the needles due to metal substitution.

In order to understand the modification introduced by Mn and Co incorporations on textural properties of goethite in detail, the specific surface area was evaluated by BET equation (from N_2 adsorption isotherms), and the results are listed in Table 1. It was found that the specific surface area of the Co containing sample was much larger than the corresponding to pure goethite (approximately 90 and 30 $m^2\,g^{-1}$, respectively). These results have been suggested by SEM images which showed that the surface/volume ratio of the observed particles increased upon introduction of Co.

Regarding the textural characteristics of α-MnFeOOH with regards to pure goethite, it could be observed that the specific surface area was increased by the substitution (see Table 1), though the textural modifications were not as important as in the case of Co-substituted sample.

Finally it is worth to note that if α-FeOOH, α-CoFeOOH and α-MnFeOOH are envisaged as supports for gold catalysts, Co(III) incorporation introduces a significant improvement in one of the characteristics of the solid, such as the specific surface area.

The thermal stability of the samples, another parameter of paramount importance regarding heterogeneous catalysts, was studied by a DTA analysis. Fig. 4 shows the profiles corresponding to α-FeOOH, α-CoFeOOH and α-MnFeOOH. It can be observed that for all the cases a main endothermic peak appears. Besides, minor peaks at lower temperature were also detected. The main peak corresponds to the dehydroxylation of goethite, leading to hematite (α-Fe_2O_3) as determined by XRD analysis of samples after performing DTA analysis.

The secondary peaks at lower temperature (at approximately 215 and 240 °C for pure goethite) than the main peak would be due to the dehydroxylation of crystals with relatively small size.

Thus the presence of multiple peaks in the DTA profiles suggests polycrystallinity.

Besides, the presence of Mn in goethite weakens and broadens the endothermic features suggesting that polycrystalinity and crystal defects are increased upon the incorporation of Mn.

The reducibility of the different samples was analyzed by TPR.

The reduction profiles of the oxyhydroxides prepared in this work are shown in Fig. 5. As can be seen, all of them present three main peaks that are named as α, β and γ. In order to describe the reduction process involved in the different profiles it should be considered that the reduction of goethite proceeds in a stepwise manner:

$$2\alpha\text{-FeOOH} \rightarrow Fe_2O_3 + H_2O \quad (1)$$

$$3Fe_2O_3 + H_2 \rightarrow 2Fe_3O_4 + H_2O \quad (2)$$

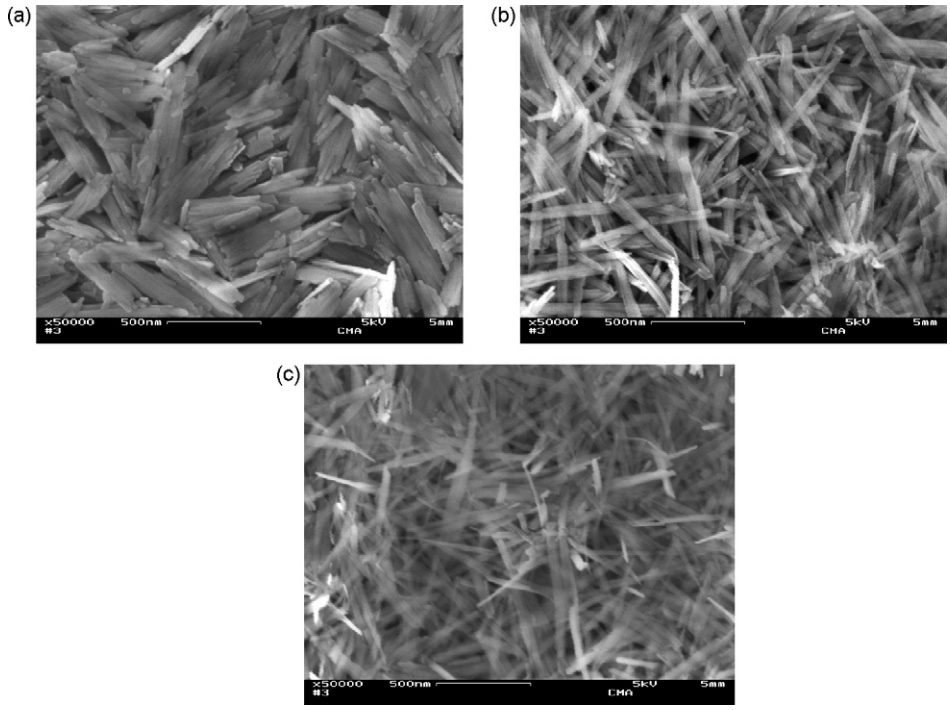

Fig. 3. SEM images for α-FeOOH(a), α-MnFeOOH (b) and α-CoFeOOH (c).

$$Fe_3O_4 + H_2 \rightarrow 3FeO + H_2O \quad (3)$$

$$FeO + H_2 \rightarrow Fe + H_2O \quad (4)$$

Reaction (1) represents the thermal decomposition of goethite to hematite, which is not detected in TPR experiments since no hydrogen consumption is accomplished for this case. The second step (2) is the reduction of hematite to magnetite while the following one represents the reduction to wüstite. Finally the total reduction to metallic Fe occurs (4).

We have made an attempt to perform a generalized description of the TPR profiles shown in Fig. 5, taking into account both the reduction reactions (chemical control) and the fact that the gaseous reactant has to be transported from the bulk gas phase to the outer surface of the crystals, followed by diffusion through the porous solid phase to the nearest interface (diffusion contribution). The α peak would be originated by the reduction (2). For all the samples, the consumption of hydrogen associated with this peak is around half the amount needed to the total reduction to magnetite. The explanation for this incomplete consumption would be related to the fact only a superficial reduction to magnetite takes place, the core of the crystal being unreduced. Regarding this point, the kinetic study made for Munteanu et al. [29] concluded that the hydroxyl groups attached to the surface provoke a decrease on the activation energy of the process of goethite reduction to magnetite.

The peaks registered at higher temperature (β and γ) would correspond to the reduction of the remnant of hematite to magnetite. For the case of the FeOOH and CoFeOOH samples the ratios between real and theoretical H_2 consumptions are approximately the unity, showing that the present results are in agreement with previous published ones [30]. For MnFeOOH

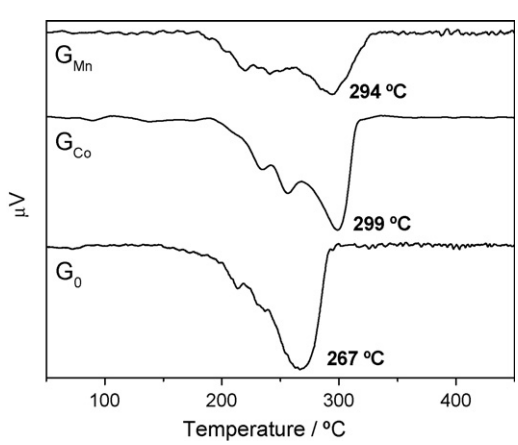

Fig. 4. DTA traces for α-FeOOH (G_0), α-MnFeOOH (G_{Mn}) and α-CoFeOOH (G_{Co}).

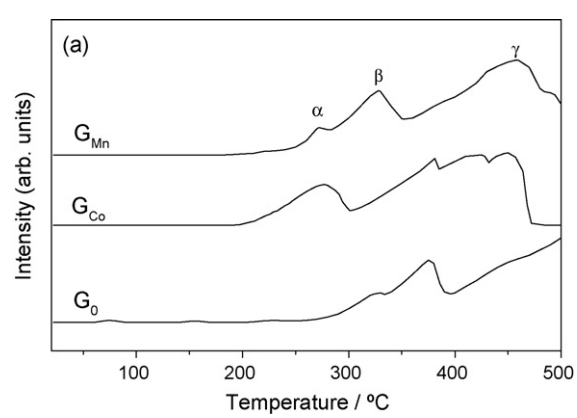

Fig. 5. TPR profiles of α-FeOOH (G_0), α-MnFeOOH (G_{Mn}) and α-CoFeOOH (G_{Co}).

the consumption was relatively high. Thus one could argue that further reduction to wusite or even to metallic iron could be accomplished for this substituted oxide.

The comparison between the profile corresponding to pure goethite with those of substituted solids indicates that the substitution with Mn or Co increases the reducibility of the goethite: the α and β peaks were displaced at lower temperature. The shift in the reduction temperature would not be related with a difference in the textural properties of samples (diffusion control), but with a modification of the chemical properties of the systems. This conclusion is based on the fact that pure goethite and Mn-substituted goethite present approximately the same specific surface are and pore volume, but a difference in the temperature ascribed to the first reduction process.

Summing up, Mn substitution originates a significant distortion of the goethite structure and a slight increase in specific surface area. On the other hand, Co substitution gives rise to a more compact goethite structure, with a large increase of the specific surface area. Both Mn(III) and Co(III) incorporation in goethite framework increase the thermal stability as well as the reducibility of the solid.

3.2. Supporting gold nanoparticles on FeOOH, α-MnFeOOH and α-CoFeOOH

The incorporation of gold to goethite was carried out following DAE method, which has been successfully employed for supporting gold nanoparticles onto alumina surface [31]. This preparation method was selected against the more conventional ones (deposition-precipitation, impregnation, co-precipitation) since goethite fulfills with all the conditions required for a successful application of DAE method. In this procedure, an aqueous $HAuCl_4$ solution (pH 3) is contacted with goethite. The surface of goethite is charged due to its anphoteric character [32]. At pH lower than the isoelectric point (IEP) of the oxide, the surface of goethite is positively charged. Taking into account that IEP of goethite is approximately 7 for goethite [33], and that the gold precursor in aqueous solution is the charged complex $[AuCl_x(H_2O)_y]^-$, the conditions for the anchoring of gold species onto the support surface are fulfilled.

In Table 1 the gold content of the samples is reported. The amount of fixed gold was relatively high for α-MnFeOOH and α-CoFeOOH since approximately the whole of the gold solution loading was irreversibly anchored to these solids. On the other hand for pure goethite, it could be considered that the method was quite ineffective since nearly 50% of the gold was not retained by the solid. We suppose that this difference could be ascribed to the different surface area of the goethites: the higher the specific surface area, the higher the loading of fixed gold.

Regarding the specific surface area, the results corresponding to Au/FeOOH, Au/α-MnFeOOH and Au/α-CoFeOOH are reported in Table 1. It is interesting to observe that a slight decrease in BET surface area arose after introducing gold to iron hydroxides.

The FT-IR spectra of Au/α-FeOOH, Au/α-MnFeOOH and Au/α-CoFeOOH are shown in Fig. 6(b). For the sake of comparison the spectra corresponding to the supports before introducing gold are also shown (see Fig. 6(a)). The bands observed at 3140 cm^{-1} are assigned to O–H stretching vibrations. The water bending band at 1650–1653, and the hydroxyl deformation band at 889–893 cm^{-1} were also observed. The bands at wavenumber lower than 700 cm^{-1} are due to lattice vibrations of the FeO_6 octahedra; the 640–635 bands are attributed to FeO_6 vibration in the a plane [34,35]. The discussion of the spectra will be focused on the OH region since they are the possible linkage sites of the $HAuCl_4$.

A slight shift to lower wavenumber of the OH stretching vibration is observed in G_{Mn}, which suggests a change in the OH characteristics due to Mn incorporation.

Upon Au incorporation, an augmentation in the intensity of the band at 3140 cm^{-1} was detected for all the cases. The OH groups concentration increase would be due to the presence of gold. We will revert to this matter latter, when discussing TPR results.

Let us pay attention to the modification of TPR profile by the presence of gold on the goethite surface. Fig. 7 shows the TPR results corresponding to Au/α-FeOOH, Au/α-MnFeOOH and Au/α-CoFeOOH.

The first consumptions (α and β peaks) were shifted to lower temperatures for the three gold containing samples in

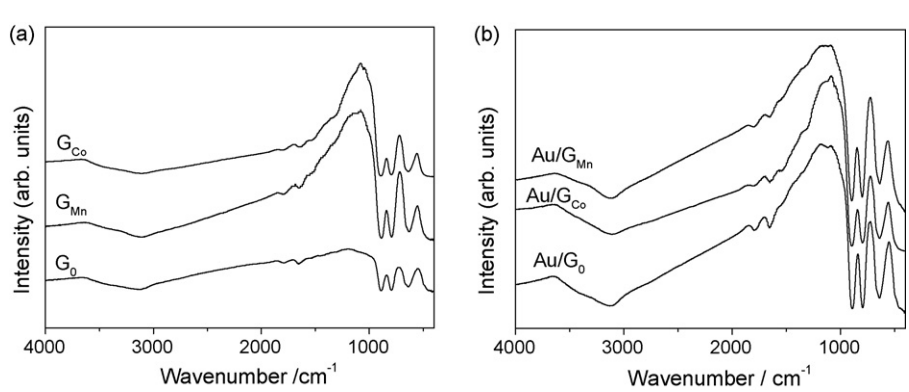

Fig. 6. (a) FT-IR spectra of α-FeOOH (G_0), α-MnFeOOH (G_{Mn}) and α-CoFeOOH (G_{Co}). (b) FT-IR spectra of Au/α-FeOOH (Au/G_0), Au/α-MnFeOOH (Au/G_{Mn}) and Au/α-CoFeOOH (Au/G_{Co}).

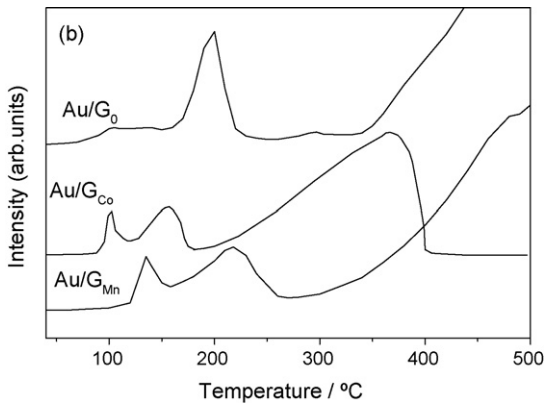

Fig. 7. TPR profiles of Au/α-FeOOH (Au/G_0), Au/α-MnFeOOH (Au/G_{Mn}) and Au/α-CoFeOOH (Au/G_{Co}).

comparison with the bare supports. The quantification of the hydrogen uptake of these peaks was slightly superior than necessary amount for transform the whole sample from goethite to magnetite (see second column in Table 1). We suggest that this increase in the amount of hydrogen consumed by the goethite would be attributed to a hydroxylation of the surface promoted by the presence of gold, in agreement with the conclusion of Ilieava et al. [36]. This behavior would be due to the presence of well-dispersed gold nanoparticles, which have the ability of dissociate water and create hydroxylated iron species according to the scheme:

$$\mathrm{Au{\cdot}O^{2-}Fe^{3+}} \xrightarrow{H_2O \,\downarrow\, H^+OH^-} \mathrm{Au{\cdot}OH^-Fe^{3+}OH^-} \xrightarrow{H_2 \,\downarrow\, H} \mathrm{Au{\cdot}Fe^{2+}OH^-{\cdot}xH_2O} \quad (5)$$

In an additional experiment, Au/α-CoFeOOH goethite was reduced under TPR experiment conditions from room temperature to 120 °C, thus the only consumption was the corresponding to α peak. This sample was characterized by XRD and the corresponding diffraction pattern indicated the presence of magnetite. Thus in this case, the reduction of goethite to magnetite is completely achieved at lower temperature than in the case of Au free goethites. This fact could be due to an electron migration favored by the gold incorporation.

Au/α-CoFeOOH was completely reduced to Fe^0, as deduced from the total hydrogen consumption reported in the last column of Table 1. The combined effect of cobalt and gold species has a huge promoter influence over all the reduction processes.

In the present work Au/goethite are envisaged to be applied in heterogeneous catalysis field, the implication being that gold should be present in the form of nanostructures on the goethite surface. For this reason, gold particle size was studied by TEM analyses of the prepared samples. The TEM study indicated that the size of these gold crystals is in the nanometric range. A relative narrow range of particle size was obtained. In Fig. 8(a) the histogram corresponding to the TEM analysis of Au/α-FeOOH is reported.

Since the stability of the gold nanostructures is of paramount importance to use Au/goethite as a catalyst in reaction at different temperatures, the TEM analysis was also performed over the Au/α-FeOOH sample reduced at 150 °C under H_2 flow. The particle size distribution is presented in Fig. 8(b). It is interesting to note that no appreciable growth of gold particles was detected, since only the crystals with sizes lower than 2 nm disappeared.

TEM analysis of Au/α-MnFeOOH also showed a narrow distribution in gold particle size, the mean diameter being 3–4 nm (Fig. 9(a)).

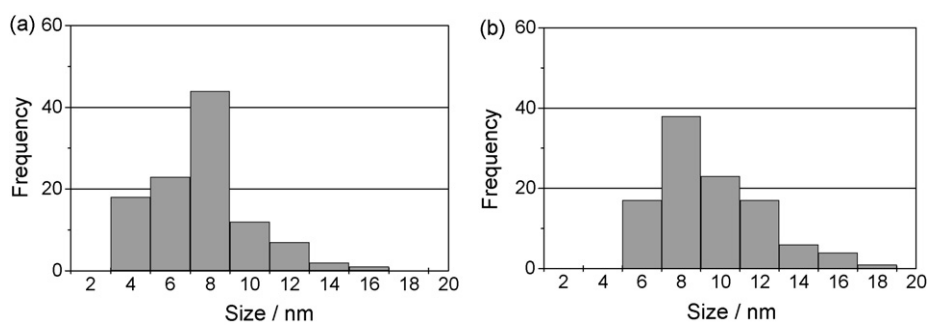

Fig. 8. (a) Particle size distribution (from TEM analysis) of Au/α-FeOOH. (b) Au/α-FeOOH following a reducing treatment.

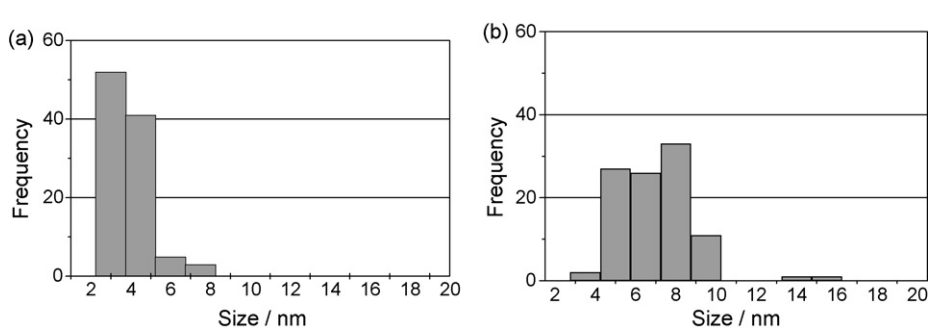

Fig. 9. (a)Particle size distribution (from TEM analysis) of Au/α-MnFeOOH. (b) Au/α-CoFeOOH.

Fig. 10. TEM image corresponding to Au/α-MnFeOOH.

To illustrate the gold particles crystals and the size of α-MnFeOOH acicular crystals, the corresponding TEM image is shown in Fig. 10. It is shown that the most part of goethite crystals are in the 30–60 nm range.

On the other hand, for Au/α-CoFeOOH a wider distribution of size was detected. The corresponding gold particle histogram is shown in Fig. 9(b). Though the most part of metal particles are lower than 10 nm, some particles are quite large (14–16 nm) and would be inactive from a catalytic point of view [1,3].

The whole of TEM results show that, though for all the studied oxides stable gold nanostructures can be obtained, the nature of the goethite has an influence in the size and distribution of gold particle.

4. Conclusion

It is possible to support gold nanoparticles on the surface of α-FeOOH and the correspondings Mn- and Co-substituted oxyhydroxides. α-MnFeOOH and α-CoFeOOH would be better supports for gold catalyst than pure goethite, since the thermal stability, the reducibility, the specific surface area and the gold loading corresponding to the formers oxides are higher than for the latter solid.

References

[1] G.J. Hutchings, J. Catal. 292 (1985) 292.
[2] M. Haruta, T. Kobayashi, H. Sano, N. Yamada, Chem. Lett. (1987) 405.
[3] G. Hutchings, M. Haruta, Appl. Catal. A 291 (2005) 2.
[4] P.A. Sermon, G. Bond, P. Wells, J. Chem. Soc., Faraday Trans. 1 (75) (1979) 385.
[5] M. Haruta, S. Tsubota, T. Kobayashi, H. Kageyama, M.J. Genet, B. Delmon, J. Catal. 144 (1993) 175.
[6] M. Haruta, Catal. Today 178 (1997) 566.
[7] M. Schubert, S. Hackenberg, A. van Veen, M. Muhler, V. Plzak, J. Behm, J. Catal. 197 (2001) 113.
[8] H. Sakurai, A. Ueda, T. Kobayashi, M. Haruta, Chem. Comunn. (1997) 271.
[9] A. Venugopal, M. Scurrell, Appl. Catal. A: Gen. 258 (2004) 241.
[10] C. Milone, R. Ingoglia, A. Pistone, G. Neri, F. Frusteri, S. Galvagno, J. Catal. 222 (2004) 348.
[11] P. Landon, P.J. Collier, A.F. Carley, D. Chadwick, A.J. Papworth, A. Burrows, C.J. Kiely, G.J. Hutchings, Phys. Chem. Chem. Phys. 5 (2003) 1917.
[12] J.K. Edwards, B. Solsona, P. Landon, A.F. Carley, A. Herzing, M. Watanabe, C.J. Kiely, G.J. Hutchings, J. Mater. Chem. 15 (2005) 4595.
[13] R. Lim-Nuñez, R.J. Gilkes, Proceedings of the International Clay Conference, Denver, USA, 1985.
[14] N. Bousserrhine, U.G. Gasser, E. Jeanroy, J. Berthelin, Geomicrobiol. J. 16 (1999) 245.
[15] J. Gerth, Geochim. Cosmochim. Acta 54 (1990) 363.
[16] M. Alvarez, E.H. Rueda, E.E. Sileo, Chem. Geol. 231 (2006) 288.
[17] D.G. Schulze, Clay Clay Miner. 32 (1984) 36.
[18] B. Campo, M. Alvarez, C. Gigola, C. Petit, E. Rueda, M. Volpe, Catal. Today (2007), doi:10.1016/jcattoday.2007.11.043.
[19] X. Sun, H.E. Doner, M. Zavarin, Clay Clay Miner. 47 (1999) 474.
[20] C. Milone, C. Gangemi, G. Neri, A. Pistone, S. Galvagno, Appl. Catal. A: Gen. 211 (2001) 251.
[21] C. Milone, R. Ingoglia, A. Pistone, G. Neri, S. Galvagno, Catal. Lett. 87 (2003) 201.
[22] W. Stiers, U. Schwertmann, Geochim. Cosmochim. Acta 49 (1985) 1909.
[23] U. Schwertmann, R.M. Cornell, Iron Oxides in the Laboratory, 2nd edn., Wiley-VCH, Weinheim, 2000.
[24] S. Ivanova, V. Pitchon, C. Petit, Appl. Catal. A 264 (2004) 197.
[25] S. Brunauer, P.H. Emmett, E. Teller, J. Am. Chem. Soc. 60 (1938) 309.
[26] R.D. Shannon, C.T. Prewitt, Acta Crystallogr. B 25 (1969) 925.
[27] E.E. Sileo, M. Alvarez, E.H. Rueda, Int. J. Inorg. Mater. 3 (2001) 2.
[28] U.G. Gasser, E. Jeanroy, C. Mustin, O. Barres, R. Nuesch, J. Bethelin, A.J. Herbillon, Clay Miner. 31 (1996) 465.
[29] G. Munteanu, L.I. Ilieva, D. Andeeva, Thermochim. Acta 291 (1997) 171.
[30] C. Milone, R. Ingoglia, L. Schipilliti, C. Crisafulli, G. Neri, S. Galvagno, J. Catal. 236 (2005) 80.
[31] S. Ivanova, V. Pitchon, C. Petit, H. Herschbach, A. Dorsselaer, E. Leize, Appl. Catal. A: Gen. 298 (2006) 203.
[32] R.M. Cornell, U. Schwertmann, The Iron Oxides. Structure, Properties, Reactions, Occurrence and Uses, Wiley-VCH, Weinheim, Germany, 1996, 573 pp.
[33] E. Tipping, D. Cooke, Geochim. Cosmochim. Acta 46 (1982) 75.
[34] P. Cambier, Clay Miner. 21 (1986) 191.
[35] P. Cambier, Clay Miner. 21 (1986) 201.
[36] L.I. Ilieva, D.H. Andreeva, A.A. Andreev, Thermochim. Acta 292 (1997) 169.